Check for updates

Engineering colloidally stable, highly fluorescent and nontoxic Cu nanoclusters *via* reaction parameter optimization†

Kumar Babu Busi,[a] Jyothi Kotha,[b] Shamili Bandaru,[a] Jyothi Priyanka Ghantasala,[b] Sheik Haseena, [a] Keerti Bhamidipati,[c] Nagaprasad Puvvada,[cd] Mahesh Kumar Ravva, [a] Manjunatha Thondamal[b] and Sabyasachi Chakrabortty [*a]

Metal nanoclusters (NCs) composed of the least number of atoms (a few to tens) have become very attractive for their emerging properties owing to their ultrasmall size. Preparing copper nanoclusters (Cu NCs) in an aqueous medium with high emission properties, strong colloidal stability, and low toxicity has been a long-standing challenge. Although Cu NCs are earth-abundant and inexpensive, they have been comparatively less explored due to their various limitations, such as ease of surface oxidation, poor colloidal stability, and high toxicity. To overcome these constraints, we established a facile synthetic route by optimizing the reaction parameters, especially altering the effective concentration of the reducing agent, to influence their optical characteristics. The improvement of the photoluminescence intensity and superior colloidal stability was modeled from a theoretical standpoint. Moreover, the as-synthesized Cu NCs showed a significant reduction of toxicity in both *in vitro* and *in vivo* models. The possibility of using such Cu NCs as a diagnostic probe toward *C. elegans* was explored. Also, the extension of our approach toward improving the photoluminescence intensity of the Cu NCs on other ligand systems was demonstrated.

1. Introduction

Noble metal nanoclusters (NCs) have attracted great attention compared to their conventional counterparts due to their ability to alter and tune properties. In particular, photoluminescence (PL) has emerged as one of the important characteristics of metal NCs.[1–3] Several potential applications are envisioned in the fields of superior biological imaging agents, sensors, photocatalytic centers, light-emitting devices, photosensitizers, *etc.*[4–6] Being extremely small with several tens of metal atoms, these clusters show properties similar to molecules without exhibiting the characteristic surface plasmon properties of relatively large metal nanoparticles (NPs).[7] It is believed that the ultrasmall core size imparts quantum effects on NCs and their subsequent optical phenomenon. They can be designed to possess good photostability, a larger Stokes shift, better

a Department of Chemistry, SRM University AP Andhra Pradesh, Andhra Pradesh 522240, India. E-mail: sabyasachi.c@srmap.edu.in

b Department of Biological Sciences, SRM University AP Andhra Pradesh, Andhra Pradesh 522240, India

c Applied Biology Division CSIR-Indian Institute of Chemical Technology, Hyderabad 500007, Telangana, India

d Department of Chemistry, Indrashil University, Rajpur, Mehsana-382740, Gujarat, India

† Electronic supplementary information (ESI) available. See https://doi.org/10.1039/d2ra02819k

photocatalytic properties, superior biocompatibility, improved colloidal stability, *etc.*, which enable their use as better diagnostic agents.[8] Compared to traditional other PL materials, such as quantum dots or organic dyes, the main advantage of NCs is related to toxicity and PL stability issues.[9,10] Moreover, the satisfactory renal clearance of metal NCs make them a better candidate for bioapplications.[11] However, they suffer from a poor fluorescent quantum yield (QY).[12] A limited number of optimized strategies are available to control their optical properties. A number of approaches such as alloy formation, aggregation-induced emission, confined fluorescence enhancement, and rigidifying the ligand shell have been employed to improve the QYs of metal NCs.[13] Several factors, such as the metal composition, surface modification, hydrophilic nature, surface charge, intrinsic structure, and the local environment, may influence their PL behavior. However, a generalized concept for QY improvement that could be applied to any composition of metal NCs has not yet been established.

Among all the studied metal NCs, gold NCs and silver NCs[14,15] have been extensively researched in terms of their size-controlled synthesis, intermetallic reaction mechanism, structural characterization, ligand-induced optical behavior, property, biological applications, catalytic performance, *etc.*[16,17] Comparing them with other metal NCs, their better conductivity, much lower cost, and earth abundancy have made Cu NCs

a popular/alternative choice in application in many industries.[18] Still, attention toward the development of Cu NCs is relatively rare owing to the difficulty in preparing small clusters and due to their susceptibility to be easily oxidized. In the literature, a series of scaffolds or capping agents, such as polymers, oligonucleotides, small molecules, proteins, and peptides, have been employed to synthesize Cu NCs successfully.[19] Among these, protein-directed synthesis is more popular as due to its environmentally benign and biocompatible nature.[20] Along with the combination of strong reducing small molecules, proteins can serve as a better surface passivating agent toward the colloidal stability of as-synthesized fluorescent Cu NCs in an aqueous medium. However, the effect of time, temperature, pH, and relative amount on their PL behavior is not yet well understood. Also, their relatively poor stability in aqueous medium due to surface oxidation and irreversible aggregation reduce their PL intensity, and hence the subsequent applications related to luminescent NCs have been curtailed to date.[21] Post-synthetic modification with electron-rich ligands was established to achieve a better stability, although this method was time-consuming and complicated.[22] Therefore, there is an utmost necessity for a robust Cu NCs synthesis protocol for retaining their strong PL intensity and superior colloidal stability, which could offer a better solution for the drawbacks to be overcome.

The wavelength region ~630 nm to 1350 nm of the electromagnetic spectrum is commonly known as the "diagnostic window" due to its several advantages over the visible range in a bioimaging context.[23] First, photons in the visible range cannot penetrate deep into the tissue due to the scattering and presence of high-level endogenous absorbers, such as lipids, hemoglobin, and water.[24] Second, elimination of the background signal, such as tissue autofluorescence, in the imaging can be achieved in this region, where the absorption coefficients of the body fluids are at their minimum.[25] Thus, this regime provides benefits toward several biological studies, such as *in vivo* and *in vitro* imaging and labeling, deep tissue imaging, and photodynamic therapy.[26] Therefore, the development of red-emitting stable, nontoxic Cu NCs as a model fluorescent probe would be of great interest.

Metallic Cu or its ionic form has much biological relevance, such as in transcriptional regulators, storage, cell surface compartment transporter and receptors, oxidoreductase behavior, free radical scavenging, and electron transfer.[27] Also, Cu is known to be removed easily from the body. However, the evaluation of such materials in both *in vivo* and *in vitro* environments would enhance their potential for translational research. In that respect, the roundworm *Caenorhabditis elegans* (*C. elegans*) has emerged as a powerful tool to assess the toxicity and biocompatibility of various chemical compounds, including nanomaterials.[28] Low-cost maintenance and ease of performing experiments have seen *C. elegans* favored over other model systems to evaluate novel nanomaterials for various biomedical applications.[29] Also, its short lifespan (average of 3 weeks) enables its use as an ideal model organism to study the effect of nanomaterials in the aging process.[30] Hence, we sought to understand the toxicity and fluorescent properties of Cu NCs in *C. elegans*.

The creation of appreciable PL with superior stability as well as involving a relatively less studied coinage metal suggest that Cu NCs would be an excellent candidate for an alternative diagnostic probe. Herein, a facile synthetic strategy to obtain highly luminescent Cu NCs was demonstrated. A clear understanding of their optical properties was well documented, where the influence of the reaction parameters on the outcome was analyzed. We believe that the reduction of the amount of the reducing agent played a crucial role in not only their enhanced PL behavior but also in their exceptional stability. To the best of our knowledge, the reported colloidal stability and quantum yield of our as-synthesized Cu NCs are the highest reported in the literature to date, where the emission wavelength is in the red region. A theoretical model was established to understand the effect of the reducing agent on the surface of Cu NCs and their effective surface passivation. Subsequently, their usefulness as diagnostics probes in *in vitro* and *in vivo* model systems was thoroughly investigated. We further showed that our approach could be extended to other synthetic conditions as well, where the varied concentration of reducing agent might lead to altering the PL intensity of Cu NCs.

2. Results and discussion

2.1 Synthesis and characterization of the Cu nanoclusters

The synthesis of Cu NCs was carried out *via* an optimized protocol based on the literature.[31] A detailed schematic showing each step together with digital images of the structures is in Scheme 1. Initially, 5 mM of copper salt ($CuSO_4$, $5H_2O$) was mixed with 150 mg of bovine serum albumin (BSA) protein in 5 mL of water. The pH of the solution was adjusted to 9 with the help of NaOH (1 M) solution before introducing a second reducing agent, *i.e.*, 25 μL of N_2H_4 solution. Finally, the reactants were allowed to react for 75 min at 55 °C under continuous stirring, to obtain colloidally stable, high luminescent Cu NCs. We carefully excluded the addition of other strong reducing agents, such as $NaBH_4$ in this case, as they might lead to the formation of larger nanoparticles in no time (Fig. S1†). The process of stabilizing Cu^{2+} ions in the aqueous medium and their subsequent Cu NCs formation is depicted in Scheme 1(b). Various functional groups on the protein backbone, $-NH_2$, $-COOH$, $-OH$, and $-SH$, were coordinated[32] with the Cu^{2+} ion to form a white colored gel, and at pH 9, they became a colloidally stable colorless solution. Finally, the initiation of Cu NC formation was started with the help of N_2H_4 solution, and after 75 min, a yellow color solution confirmed their successful synthesis. This process was relatively simple and robust. As seen in the digital image (Scheme 1(b)), BSA-stabilized Cu NCs showed a nice dispersion in aqueous medium and a light yellow color. The BSA-stabilized Cu NCs were purified through a Viva-spin 20 (MWCO30k) centrifugal concentrator to remove unreacted small molecules used in the synthesis. Here, we assume statistically that all the BSA molecules were attached with Cu NCs. Further, they were analyzed by UV-Vis absorption,

photoluminescence, and other advanced characterization techniques.

Optical and structural characterizations of the as-synthesized Cu NCs are depicted in Fig. 1. No sharp absorbance peak was observed for Cu NCs, which eliminated the possibility of the formation of larger-sized Cu nanoparticles that generally originate through surface plasmon resonance at ~540 nm (Fig. S1†). It was observed that these NCs showed the highest excitation peak at ~390 nm and emission maximum at ~650 nm (Fig. 1(a)). This larger Stoke's shift between the excitation and emission behavior could be very beneficial for further bioimaging applications, as the incoming excitation source would have minimal interaction with the emission detector. Also, red/near infrared emission is advantageous in bioimaging where deep tissue penetration is necessary. To understand the nature of the emission peak, we excited the Cu NCs samples under various excitation sources, ranging from 300 to 480 nm. A clear excitation independent PL profile was recorded where the emission peak was not shifted (Fig. 1(b)). However, the observed intensities were varied depending on their absorption cross-section. Taken together, we can conclude that better surface passivation was achieved with minimal occurrence of surface defects despite the extremely small regime. A digital image (Fig. 1(c)) showed that the as-synthesized Cu NCs were yellowish in color under room light and emitted red color under UV light irradiation (365 nm). From dynamic light scattering (DLS) experiments, we observed that the hydrodynamic diameter of these Cu NCs was ~4.7 nm, which is similar to BSA protein itself, and no other aggregates were found. The capping layer of BSA was useful for the prevention of agglomeration in water. These NCs were

colloidally stable, and had a zeta potential value of ~−27.99 mV, which clearly indicated their stability in aqueous medium. This could be beneficial for their use in bioimaging applications. A high-resolution transmission electron microscopy (HRTEM) image of such Cu NCs is presented in the inset of Fig. 1(d), where the crystalline nature of the NCs was clearly evident. The calculated lattice spacing of 0.207 nm confirmed the existence of the Cu (111) plane[33] in their structure. Their average size was calculated to be 2.2 ± 0.2 nm, which was obtained after careful consideration of ~40 representative such small NCs in the TEM images (Fig. 1(d)). Size comparisons of Cu NCs measured from TEM and DLS measurements were carried out to show that both sizes were well correlated and matched. The slight increase in the hydrodynamic size compared to the projected size might be ascribed to the presence of ligand shell/functional groups on the surface of nanoparticles in the aqueous state, which is a well-accepted proposition for colloidal stability. To understand the surface chemical state of the NCs, X-ray photoelectron spectroscopy (XPS) characterization was performed. The initial survey spectrum (Fig. 1(e)) revealed the presence of C, N, S, and O atoms, which generally originated from the BSA protein backbone present with the Cu NCs. A closer analysis of the binding energy peaks near the Cu atoms revealed the existence of 932.9 and 953 eV peaks for Cu-$2p_{3/2}$ and Cu-$2p_{1/2}$ respectively. However, the absence of a 942 eV peak confirmed the non-appearance of Cu^{2+} peaks, proving all the Cu^{2+} precursors were completely reduced in our reaction condition to produce Cu NCs. Also, C 1s peak analysis of BSA-Cu NCs showed three peaks corresponding to C=C or C–C (284.79 eV), C–C/COOH/C–N (285.99 eV), and C=O/C=N (287.84 eV), respectively (Fig. S2(a)†). Similarly, the N 1s peaks confirmed

Scheme 1 (a) Schematic illustration of Cu NCs synthesis through a simple, optimized chemical reduction method, where N_2H_4 was used as a secondary mild reducing agent. (b) Digital images of glass vials demonstrating the formation of Cu NCs inside the colloidal solution *via* a step-by-step process.
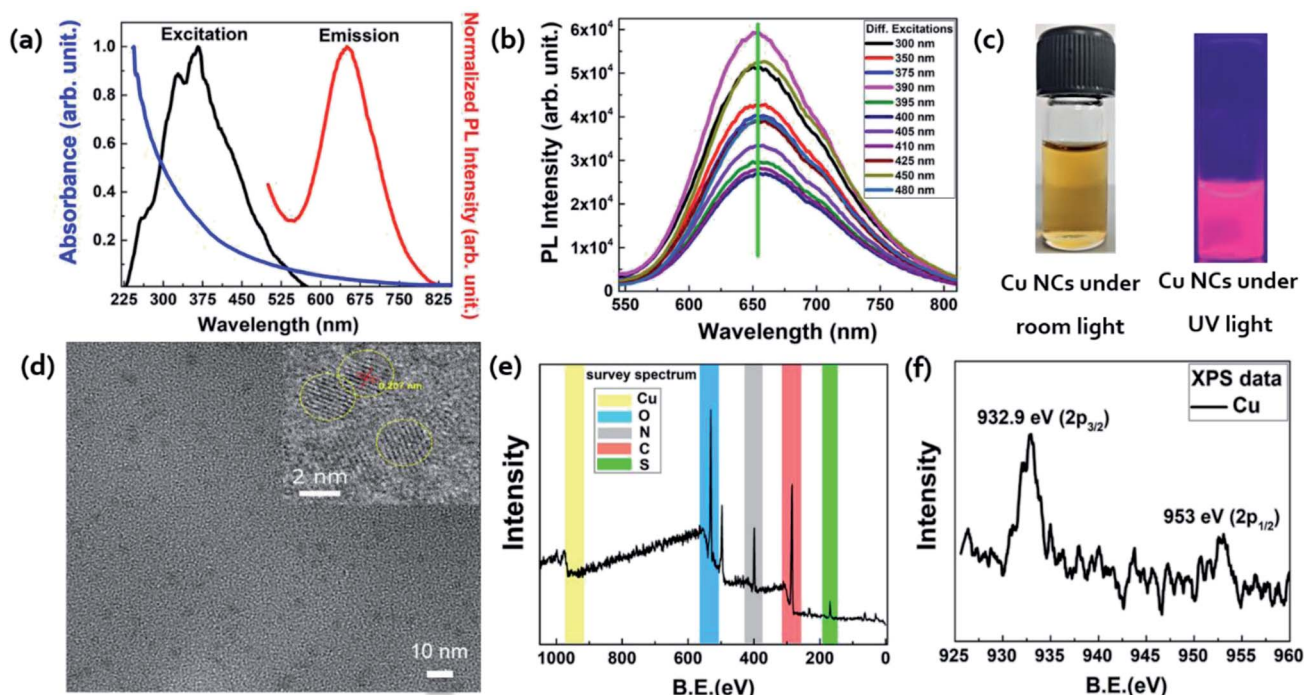
Fig. 1 (a) Typical absorbance (blue line) spectra of Cu NCs, showing there was no observable plasmon peak, demonstrating the ultrasmall size in the colloidal solution. The subsequent emission (red line) spectra were recorded in the red region at 650 nm by exciting (black line) the Cu NCs at 390 nm wavelength. (b) PL measurements of the Cu NCs recorded at different excitation wavelengths, where the maximum red emission was observed at 390 nm excitation wavelength. (c) Representative digital photographs of Cu NCs under room light exhibiting a pale yellow color, while Cu NCs exposed to UV light (365 nm) emitted an intense red color emission. (d) Typical TEM image of BSA-Cu NCs demonstrating the crystalline structure of the NCs. Cu(111) plane lattice spacing of 0.20 nm with an average size of 2.2 ± 0.2 nm shown in the inset HRTEM image. (e) Representative BSA-Cu NCs XPS full survey spectrum, (f) high-resolution XPS revealing the existence of Cu $2p_{3/2}$ and $2p_{1/2}$ binding energies attributed to Cu(0) zero-valent and Cu(+1) monovalent oxidation states.

the presence of NH_3 (400.33 eV) and CH_3–C–N (398.98 eV), whereas O 1s showed three peaks attributed to O**=C–OH (531.37 eV), O=C–O**H (532.98 eV), and O_2/C (536.98 eV) (Fig. S2(b and c)†). Taken together, all three elements confirmed the presence of a protein backbone in the as-prepared Cu NCs. We further compared the Fourier-transform infrared spectroscopy (FTIR) data of Cu-BSA and BSA alone. No observable change was observed, indicating that the Cu NCs were completely embedded inside the protein backbone (Fig. S3†) and the surface structure of BSA was largely unaltered.[31]

2.2 Improvement of the quantum yield of the Cu nanoclusters

The above-mentioned reaction conditions were thoroughly optimized through careful variation of all the parameters involved in the synthesis. The key parameters, such as temperature, time, pH, reducing agent amount, and surface capping agent, were taken into consideration to yield a better PL intensity and impart better colloidal stability. In each of the cases, there was no apparent shift in the emission peak position, clearly confirming that neither the capping layer was degraded nor was aggregation through irreversible ligand loss observed in these experimental conditions. A remarkable improvement in the quantum yield (QY) of ~7 times (from 4.1%

to 28%) was recorded under our optimum condition. Fig. 2(a–d) clearly demonstrate the change in their PL behaviors in the varied conditions (Fig. S4–S8†), where we plotted the normalized area under each PL spectra. Since, most the literature studies on protein-templated Cu NCs synthesis kept the amount of our secondary reducing agent N_2H_4 solution as 1 mL in their synthesis,[34,35] we also followed the same in our comparison study. Fig. 2(a) shows the highest PL intensity occurred at 55 °C, while comparing it with other synthesis temperatures. This could be attributed to the fact that a relatively higher energy was needed for the acceleration of the reduction dynamics of Cu^{2+} salt compared with the standard biological temperature (37 °C). However, very high temperatures led to the formation of larger-sized Cu nanoparticles (NPs) with no fluorescence emission. The optimum time to get better Cu NCs formation was recognized to be around ~75 min in Fig. 2(b). We believe this period would be sufficient to obtain better surface passivation with BSA with an appropriate size regime, while a longer time might lead to the formation of larger-sized Cu NCs with no PL emission. As pH is a vital parameter for synthesizing any nanomaterials to be used in bioapplications,[36,37] we synthesized our Cu NCs at 55 °C for 75 min under various pH conditions ranging from pH 2–12 (Fig. S6†). The better PL intensity was confirmed for the pH 9 solution, as displayed in Fig. 2(c). It was worth mentioning that our reaction condition proved to be very robust as we observed
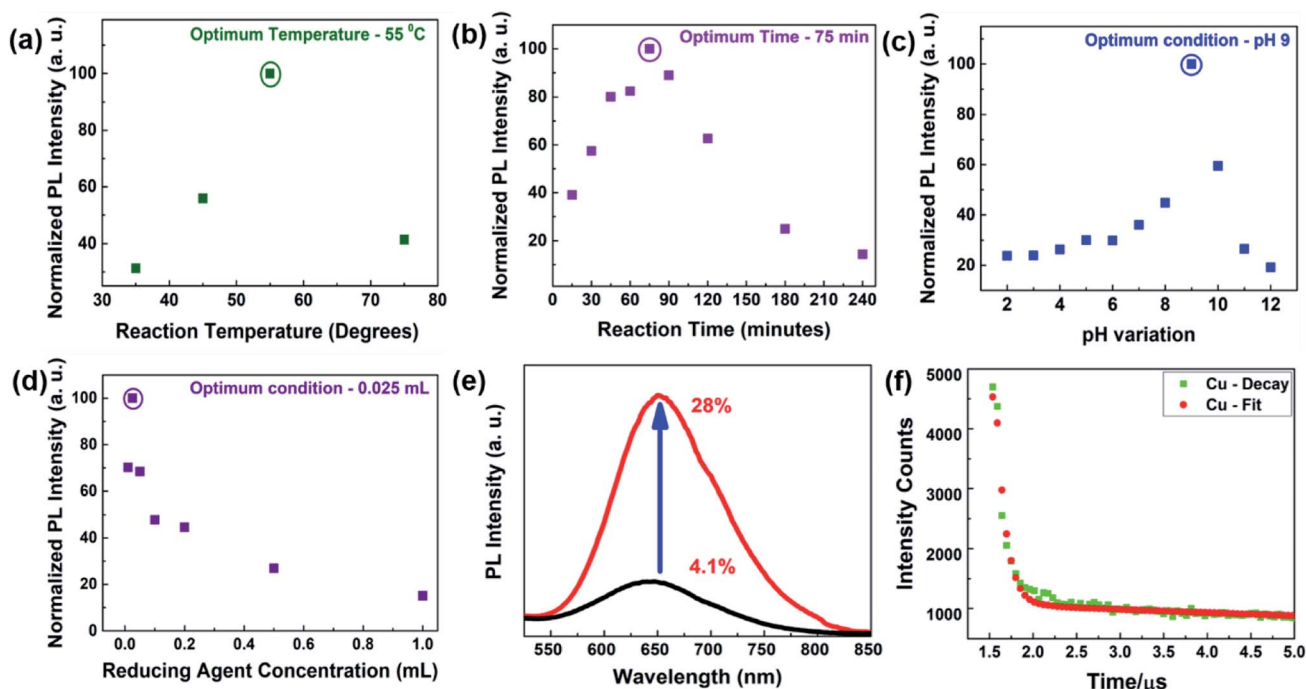
Fig. 2 Optimization of the reaction parameters for possessing high red luminescence and a better colloidal stability of our BSA-Cu NCs. Plots of the key reaction parameters: (a) reaction temperature (b) reaction time (c) pH of the solution (d) amount of secondary reducing agent. (e) Optimal reaction parameters allowed improving the QY from 4.1% to 28% for the BSA-Cu NCs. (f) Three exponential fittings of the time-resolved PL lifetime decay patterns (standard TCSPC) of optimized BSA-Cu NCs correlated to the improved QY.

appreciable PL in every pH solution. In the literature, PVP-coated Cu NCs[38] showed better PL intensity at pH 4, whereas the change in pH to 7 led to aggregation and no fluorescent was observed. Finally, we evaluated the role of reducing agents for the obtained optical behavior of Cu NCs. Interestingly, their amount was of utmost importance, and we observed better quality NCs while using 0.025 mL of N_2H_4 solution, as depicted in Fig. 2(d). To the best of our knowledge, this is the highest reported QY (∼28%) for protein-coated Cu NCs emitting around the red region (∼650 nm) of the visible spectrum, so far. Fig. 2(e) presents the change in PL intensity of the as-synthesized Cu NCs in BSA, where the amount of reducing agent was used as 1 mL and 0.025 mL in gray and red color spectra, respectively. The slight shift in PL emission peak may be attributed to the fact that amount of $-N_2H_4$ influenced the surface passivation. This observation was supported later by the radiative recombination dynamics. Fig. 2(f) shows the lifetime decay curve of the as-synthesized Cu NCs, and it was fitted with three exponential decay profiles. An average lifetime of 2.17 μs was recorded in the standard time-correlated single-photon counting (TCSPC) measurements. An improvement of ∼4 order of magnitude lifetime value was observed while comparing the PL decay of 1 mL reducing agent (Fig. S9†). We compare in Table 1 our synthesis method, reaction time, the temperature of the synthesis, capping ligand, the lifetime of as-synthesized NCs, their QYs, corresponding excitation, and emission wavelength mainly focused on red fluorescent Cu NCs with others reported in the literature. As depicted, our protocol yielded a better QY, which was further substantiated by their longest lifetime. We

believe poor passivation, increased surface trap states, or the destruction of the structural properties of the protein backbone in the case of a higher amount of reducing agent may influence their PL behavior. A further hypothesis on the effect of this low concentration of their observed PL behavior is explained through density functional theory (DFT) calculations in the next section.

2.3 Theoretical modeling of the Cu nanoclusters

In order to gain insights into the role of hydrazine on the Cu surface and the capping agent's interactions, DFT calculations were carried out by considering six model systems. Each model system consisted of a Cu (38) cluster and a small alkyl chain containing an amine and a carboxylic acid functional group to mimic the capping groups. Furthermore, to understand the impact of hydrazine molecules on the interaction between the Cu cluster and capping group, geometry optimizations of the model systems were carried out in the presence and absence of hydrazine molecules. The model systems geometries were optimized using the B3LYP method using two different basis sets, namely the LANL2DZ basis set for Cu atoms and 6-31g* basis set for C, H, N, and O atoms. The optimized geometries of the model systems considered in the study are depicted in Fig. 3. In the absence of hydrazine (Fig. 3(a)), the intermolecular distance between the nitrogen atom in amine functional group and Cu atom in the Cu cluster was ∼2.19 Å. The same value increased from 2.19 Å to 2.25 Å when more hydrazine molecules were allowed to interact with the Cu cluster.

Table 1 Comparison of the as-synthesized Cu NCs from various synthetic methods and capping ligands, where the emission was centered around the red luminescent region, as reported in the literature

Serial no.	Synthesis method	Reaction time	Temperature (°C)	Capping agent	Lifetime	QY (%)	$\lambda_{ex}/\lambda_{em}$ (nm)	Ref.
1	UV irradiation	3 h	—	Poly(methacrylic acid)	—	2.2	360/630	39
2	UV irradiation	2 h	—	Poly(acrylic acid)*graft*-mercaptoethylamine	—	5.7	365/630	40
3	Stirring	30 min	—	PVP/dihydrolipoic acid	0.8 μs	10.8	365/435 650	38
4	Stirring	4 h	55	BSA	—	4.1	365/620	31
5	Stirring	2 h	40	Lysozyme	—	5.6	365/600	41
6	Stirring	2 h	37	Papain	—	14.3	370/620	42
7	Stirring	3.5 h	25	Transferrin	15.2 ns	6.2	508/670	43
8	Shaking	—	—	Glutathione	15.2 μs	1.9	340/627	44
9	Stirring	—	RT	Glutathione	—	3	340/620	45
10	Stirring	10 min	80	Glutathione	—	5	410/610	46
11	Stirring	1 h	37	Glutathione	—	3.6	360/600	47
12	Stirring	5 h	RT	Glutathione	—	—	345/620	48
13	Stirring	90 min	RT	D-Penicillamine	150 μs	16.6	345/640	49
14	Stirring	4 h	RT	Human serum albumin	—	—	390/646	35
15	Stirring	15 min	45	Glutathione	—	2.1	394/585	50
16	Grinding	—	35	Phenylethanethiol	—	—	405/605	51
17	Stirring	5 h	RT	BSA	—	3.7	365/630	52
18	Colloidal	75 min	55	BSA	2.17 μs	**28**	375/650	**This work**[39]

Further, we calculated the binding energy (BE) between the alkyl chain and the Cu cluster with and without hydrazine molecules. As shown in Fig. 3, the calculated BE between the Cu cluster and capping group was 37.8 kcal mol^{-1} in the absence of hydrazine molecules. The same value came down to 29.08 kcal mol^{-1} when five hydrazine molecules were adsorbed on the Cu cluster surface. We observed a clear relationship between the number of hydrazine molecules adsorbed and BEs between the alkyl chain and the Cu cluster. Overall, these results clearly indicated that the introduction of more hydrazine molecules weakened the interaction between the capping groups and Cu clusters. We believe that a gradual addition or effective increase of hydrazine molecules near the Cu surface might influence the poor surface passivation and therefore open more surface trap states, which would finally lead to a QY and lifetime decrease.

2.4 Stability and cytotoxicity study of the Cu nanoclusters

Another promising phenomenon of our protocol was the exceptional stability of the as-synthesized Cu NCs. In general, literature reports stated that Cu NCs or Cu NPs were not stable under ambient conditions in the open air as they are very prone to surface oxidation, which restricts their usefulness in potential bioimaging applications. To improve their stability, various techniques, such as the addition of Zn^{2+} or S^{2-} (ref. 53) or the incorporation of pyrimidine-based ligands,[54] have been employed. Such various capping groups and their stability times are highlighted in Table 2. To the best of our knowledge, our as-synthesized Cu NCs possessed remarkable optical stability of ~6 months, where the emission intensity was found to be similar (with no peak shift) compared with the first-day sample's results (Fig. 4(a)). In addition, we observed little decrease in the emission intensity in a 10 months-old sample

(Fig. S10†). This kind of phenomenon could be further rationalized *via* their better surface passivation at the higher pH 9 in our synthesis protocol. Also at pH 9, the di-sulfide bonds in the BSA protein backbone might open, which could stabilize/passivate the cluster further through Cu–S interactions.[55]

Before evaluating the potential of the Cu NCs in bioimaging as a diagnostic probe, we assessed their stabilities under various biological media. Respective PL intensity curves were monitored to eliminate the possibilities of PL loss or aggregation under those conditions. We incubated our Cu NCs with fetal bovine serum (FBS), PBS, and RPMI 1640 media for ~6 h, and recorded the subsequent PL spectra. In all conditions, the existence of similar fluorescent intensities proved the tolerance of our NCs (Fig. S11†). Since the as-prepared Cu NCs were protected by the BSA layer, we expected them to be low or nontoxic toward cells at a suitable concentration. Thus, their toxicity evaluation (MTT assays) was performed through *in vitro* cell viability experiments, where two representative cell lines, namely HEK 293 (human embryonic kidney) and MDA-MB 231 (human breast adenocarcinoma), were employed. The Cu NCs were added to the two cancerous cell lines at various concentrations from ~0.5 μM to 100 μM. Largely, our Cu NCs largely displayed nontoxicity toward those cell lines as they maintained their normal morphology after incubation. Even at a higher concentration, such as ~100 μM Cu concentration, ~80% cells were viable, where the negative control anticancer chemotherapeutic doxorubicin (DOX) showed proficient killing of cells at ~2.5 μM concentration (Fig. 4(b and c)). Furthermore, we used confocal microscopy to investigate the intracellular uptake of tailored Cu NCs in the MDA-MB 231 cell line.[56]

Here, MDA-MB 231 adenocarcinoma cells were treated with Cu NCs at 10 μM concentration for an intracellular morphology and uptake study using a fluorescence confocal microscope as displayed in Fig. S12.† It was visibly observed that there was no
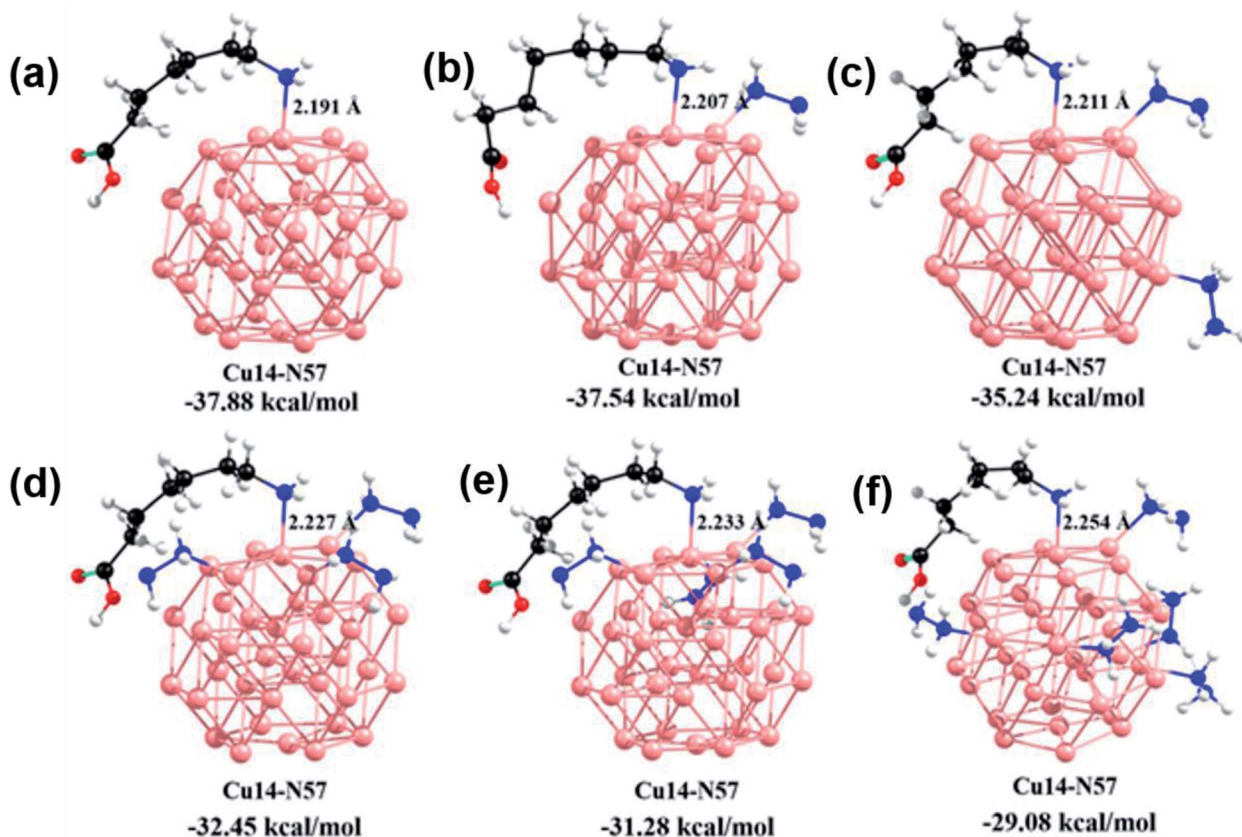
Fig. 3 Cu_{38} cluster binding with a capping agent (alkyl chain with amine and carboxylic acid functional groups) along with their intermolecular distances and binding energies in the presence of: (a) no hydrazine molecules, (b) one hydrazine molecule, (c) two hydrazine molecules, (d) three hydrazine molecules, (e) four hydrazine molecules, and (f) five hydrazine molecules.

effective change in the morphology of the MDA-MB 231 cells after the above treatments compared to the control (untreated-UT) cells. From the images, it could be clearly comprehended that the Cu NCs were localized inside the cell efficiently. The red fluorescence signal was found to be stable but relatively low at the 24 h time-point. These observations noticeably indicate the biocompatible nature and operative use of the Cu NCs compound as a fluorescence cell marker and delivery agent upon future studies (Fig. 4).

2.5 Whole-body disseminations and the effect on the life span of Cu nanoclusters on *C. elegans*

To assess whether Cu NCs possess intact fluorescent properties in biological samples, we performed *in vivo* experiments to study the biodistribution of these nanoclusters in *C. elegans*. Worms exposed to a solution of Cu NCs synthesized in a reducing agent of higher concentration died immediately (where 1 mL N_2H_4 was used for the reduction) compared to animals incubated in Cu NCs synthesized using our modified

Table 2 Colloidal stability of other red-emitting Cu NCs, reported in the literature, compared with our optimized BSA-derived Cu NCs

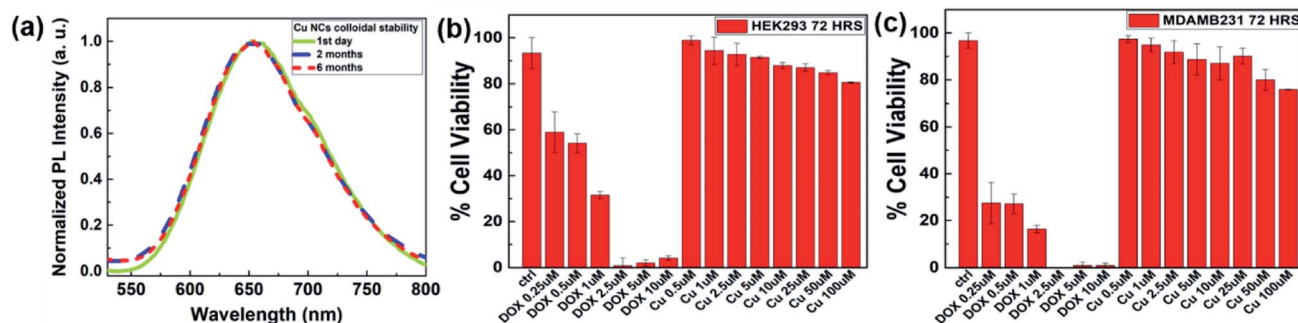| S. no.	Capping agent	$\lambda_{exc}/\lambda_{em}$ (nm)	Stability time	Ref.
1	PVP/dihydrolipoic acid	365/435 650	3 days	38
2	Egg white	395/621	48 hours	57
3	5-Methyl-2-thiouracil	402/670	3 months	54
4	Cysteine	365/660	15 days	58
5	BSA	395/645	2 months	59
6	BSA	365/630	24 hours	44
7	BSA	365/643	18 days	34
8	GSH	358/593	2 months	60
9	ssDNA	340/645	30 minutes	22
10	BSA	365/650	**6 months**	**This work**

Fig. 4 (a) Typical PL spectra corresponding to the colloidally stable Cu NCs in aqueous medium for up to 6 months without any decrease in the PL intensity. (b and c) MTT assay results to determine the viability of HEK293, MDAMB231 cells after 72 h treatment with varying concentrations of BSA-Cu NCs in the cell medium. Excellent nontoxic behavior was observed.

protocol (Fig. 5(d)), with the corresponding video given in the ESI (Fig. S13†). Hence all the subsequent *in vivo* assessments in *C. elegans* were performed with the as-synthesized Cu NCs (when 25 μL N_2H_4 was added for the reduction) and they exhibited exceptional low acute toxicity (Fig. 5(c)). The corresponding video is attached in the ESI (Fig. S14†). We first incubated worms in Cu NCs solution for various time periods. Fixed worms were imaged using fluorescent microscopy. We found strong fluorescent signals (OPTIKA B1000 fluorescent microscope ITALY 40 × 0.75 lens, excitation channel 405 nm) arising from Cu NCs accumulation in various tissues, such as the pharynx, gut, and tail region, in *C. elegans*. Interestingly, we

could not detect any signal arising from the embryos in the gonad (Fig. 5(e)).

Though several studies have reported the acute toxicity of various nanomaterials, the effect of nanoclusters on the organismal lifespan is poorly documented. To assess the effect of Cu NCs exposure on the lifespan, we scored the survivorship of *C. elegans* exposed to Cu NCs (1.25 mM for 12 h, Fig. 5(a)). We found no significant changes in the mean lifespan of animals exposed to Cu NCs as compared to animals incubated in BSA (Fig. S15†). This finding suggests that Cu NCs synthesized using the chemical reduction method and optimal N_2H_4 reducing agent concentration did not show a toxic effect on organismal
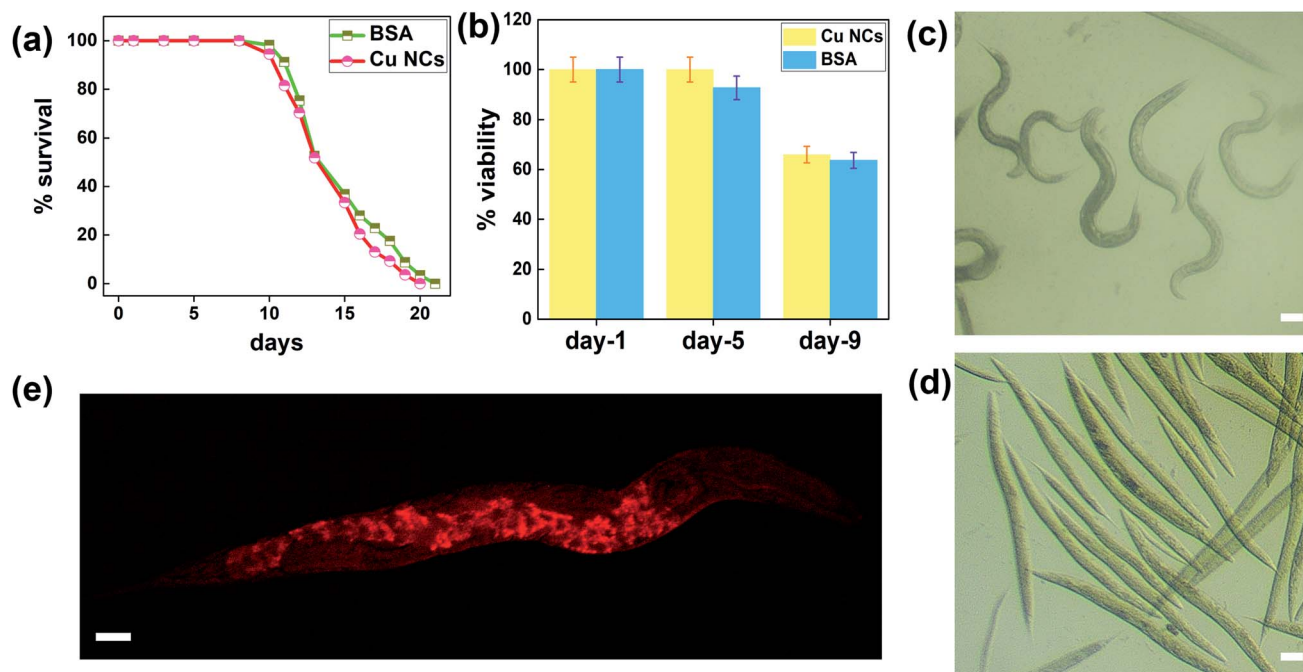

Fig. 5 *In vivo* toxicity assessment of Cu NCs in *C. elegans*: (a) *C. elegans* treated with Cu NC-I did not show any change in mean lifespan compared to worms treated with BSA as the control (*P* > 0.19). (b) Short-term exposure to Cu NC-I of 1.25 mM concentration for 4 h, which did not show any toxic effect on *C. elegans* survival. (c) Brightfield images of worms after 30 min incubation in Cu NC-I solution (c) and Cu NC-II solution. (d) Microscope image of worms incubated in Cu NCs solution for 4 h, showing the strong signal from the gut region. (e) Images obtained using an OPTIKA B1000 fluorescent microscope. Scale bar corresponds to 50 μM. Survival analysis was performed by OASIS online analysis using the lifespan assays tool.
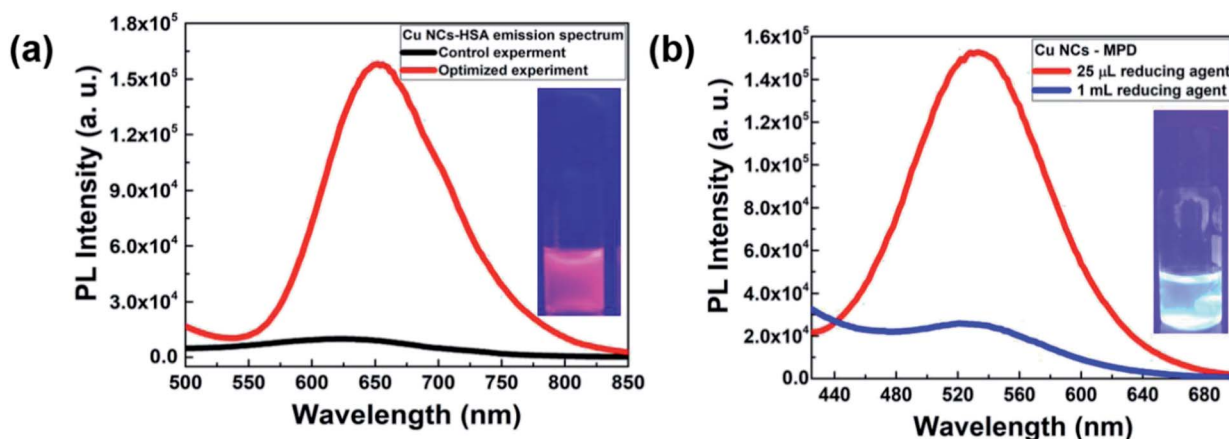
Fig. 6 (a) HSA−derived Cu NCs giving a huge increase in the PL QY with bright red luminescence in the red region at 654 nm when following the optimized protocol condition. (b) Following the same optimized protocol condition, the MPD ligand also produced brilliant green color emission for the Cu NCs at 540 nm.

survivorship (Fig. 5(b)). Taken together, these phenomena could open new possibilities of using Cu NCs as a unique diagnostic probe compared to others, such as easily photo-bleachable organic dyes, expensive noble metal NCs, and toxic Cd-based quantum dots.[10]

As copper is known for its natural antimicrobial properties, we hypothesized that the as-synthesized Cu NCs would also exhibit the same property.[61] To demonstrate this, antimicrobial assays were performed using the disk diffusion technique. The optimized Cu NCs-I exhibited excellent antimicrobial properties at higher concentrations only, due to their nontoxicity at lower concentrations not exhibiting decent antimicrobial properties (Fig. S16†).

2.6 Extension of our approach toward different reductive environments

To extend and perceive the wide applicability of our approach, we employed a similar concept to prepare Cu NCs with other ligands. Our representative candidates were other red-emitting and green-emitting Cu NCs where human serum albumin (HSA) and *meta*-phenylenediamine (MPD) were used as the primary surfactant, respectively. In both, while reducing the effective amount of the second reducing agent, *i.e.*, hydrazine to a low amount, a significant increase in emission intensity was recorded. We believe that "the reduction of the reducing agent amount" concept holds promise in other reductive environments at large for obtaining better QYs in Cu NCs preparation (Fig. 6).

3. Conclusions

In summary, a facile synthetic strategy for obtaining Cu NCs was demonstrated, where careful control over various reaction parameters was evaluated. In particular, the amount of the second reducing agent, *i.e.*, N_2H_4, played a crucial role in obtaining highly fluorescent Cu NCs. Moreover, a theoretical model was established, where more N_2H_4 could introduce

a weak interaction between the capping groups and the Cu NCs, leading to poor stability as well as a low QY. Our optimized samples showed excellent biocompatibility toward solid cancer cell lines and *C. elegans* in *in vitro* and *in vivo* environments, respectively. Taken together, the potential of such Cu NCs as a diagnostic probe was evaluated using *C. elegans* as a model organism. In particular, the as-synthesized Cu NCs with a low amount of N_2H_4 imparted almost no toxicity toward the health span of *C. elegans*. Also, these NCs showed potential in terms of an antibacterial effect, which could be explored further. Finally, successful implementation of these reaction parameters control was applied for improvement of the PL properties while synthesizing Cu NCs using another set of ligand systems. Thus, a transition from a low QY to better QY with nontoxic and colloidal stable metal nanoclusters was observed, providing an innovative way to control the reaction parameters for their use in diagnostically relevant probes in the biological environment. We believe other strategies, such as altering the surface charge, different metal compositions, various intrinsic structures, proper choice of environment, could open up avenues to explore the known methodologies with careful optimization for yielding better attributes.

Conflicts of interest

The authors declare no conflicts of interest.

Acknowledgements

References

1 Z. Lin, N. Goswami, T. Xue, O. J. H. Chai, H. Xu, Y. Liu, Y. Su and J. Xie, *Adv. Funct. Mater.*, 2021, **31**, 2105662.

2 T. Chen, H. Lin, Y. Cao, Q. Yao and J. Xie, *Adv. Mater.*, 2021, 2103918.

3 T. Higaki, Q. Li, M. Zhou, S. Zhao, Y. Li, S. Li and R. Jin, *Acc. Chem. Res.*, 2018, **51**, 2764–2773.

4 W. F. Lai, W. T. Wong and A. L. Rogach, *Adv. Mater.*, 2020, **32**, 1–21.

5 K. Zheng and J. Xie, *Trends Chem.*, 2020, **2**, 665–679.

6 A. Mathew and T. Pradeep, *Part. Part. Syst. Charact.*, 2014, **31**, 1017–1053.

7 X. Kang and M. Zhu, *Chem. Soc. Rev.*, 2019, **48**, 2422–2457.

8 K. B. Busi, M. Palanivel, K. K. Ghosh, W. B. Ball, B. Gulyás, P. Padmanabhan and S. Chakrabortty, *Nanomaterials*, 2022, **12**, 301.

9 S. Chakrabortty, J. A. Yang, Y. M. Tan, N. Mishra and Y. Chan, *Angew. Chem., Int. Ed.*, 2010, **49**, 2888–2892.

10 Y. Wu, S. Chakrabortty, R. A. Gropeanu, J. Wilhelmi, Y. Xu, K. Shih Er, S. Ling Kuan, K. Koynov, Y. Chan and T. Weil, *J. Am. Chem. Soc.*, 2010, **132**, 5012–5014.

11 C. N. Loynachan, A. P. Soleimany, J. S. Dudani, Y. Lin, A. Najer, A. Bekdemir, Q. Chen, S. N. Bhatia and M. M. Stevens, *Nat. Nanotechnol.*, 2019, **14**, 883–890.

12 Z. Wang, B. Chen and A. L. Rogach, *Nanoscale Horiz.*, 2017, **2**, 135–146.

13 S. Shahsavari, S. Hadian-Ghazvini, F. Hooriabad Saboor, I. Menbari Oskouie, M. Hasany, A. Simchi and A. L. Rogach, *Mater. Chem. Front.*, 2019, **3**, 2326–2356.

14 Y. Liu, Z. Li, W. Zhong, L. Zhang, W. Chen and Q. Li, *Nanoscale Res. Lett.*, 2014, **9**, 1–8.

15 H. Xu and K. S. Suslick, *Adv. Mater.*, 2010, **22**, 1078–1082.

16 I. Chakraborty and T. Pradeep, *Chem. Rev.*, 2017, **117**, 8208–8271.

17 J. Yang and R. Jin, *ACS Mater. Lett.*, 2019, **1**, 482–489.

18 Y. S. Lin, Y. F. Lin, A. Nain, Y. F. Huang and H. T. Chang, *Sensors and Actuators Reports*, 2021, **3**, 100026.

19 A. Baghdasaryan and T. Bürgi, *Nanoscale*, 2021, **13**, 6283–6340.

20 J. Xie, Y. Zheng and J. Y. Ying, *J. Am. Chem. Soc.*, 2009, **131**, 888–889.

21 Z. Zhao and Y. Li, *Colloids Surf., B*, 2020, **195**, 111244.

22 Z. Qing, X. He, D. He, K. Wang, F. Xu, T. Qing and X. Yang, *Angew. Chem., Int. Ed.*, 2013, **52**, 9719–9722.

23 J. Li, J. J. Zhu and K. Xu, *TrAC, Trends Anal. Chem.*, 2014, **58**, 90–98.

24 R. Datta, T. M. Heaster, J. T. Sharick, A. A. Gillette and M. C. Skala, *J. Biomed. Opt.*, 2020, **25**, 1.

25 J. M. An, S. H. Kim and D. Kim, *Org. Biomol. Chem.*, 2020, **18**, 4288–4297.

26 G. S. Heo, Y. Zhao, D. Sultan, X. Zhang, L. Detering, H. P. Luehmann, X. Zhang, R. Li, A. Choksi, S. Sharp, S. Levingston, T. Primeau, D. E. Reichert, G. Sun, B. Razani, S. Li, K. N. Weilbaecher, F. Dehdashti, K. L. Wooley and Y. Liu, *ACS Appl. Mater. Interfaces*, 2019, **11**, 19669–19678.

27 A. Dutta, U. Goswami and A. Chattopadhyay, *ACS Appl. Mater. Interfaces*, 2018, **10**, 19459–19472.

28 P. R. Hunt, *J. Appl. Toxicol.*, 2017, **37**, 50–59.

29 T. Wu, H. Xu, X. Liang and M. Tang, *Chemosphere*, 2019, **221**, 708–726.

30 M. Markaki and N. Tavernarakis, *Biotechnol. J.*, 2010, **5**, 1261–1276.

31 C. Wang, C. Wang, L. Xu, H. Cheng, Q. Lin and C. Zhang, *Nanoscale*, 2014, **6**, 1775–1781.

32 R. Singh, S. Majhi, K. Sharma, M. Ali, S. Sharma, D. Choudhary, C. S. P. Tripathi and D. Guin, *Chem. Phys. Lett.*, 2021, 139226.

33 N. Goswami, A. Giri, M. S. Bootharaju, P. L. Xavier, T. Pradeep and S. K. Pal, *Anal. Chem.*, 2011, **83**, 9676–9680.

34 R. Rajamanikandan and M. Ilanchelian, *Anal. Methods*, 2018, **10**, 3666–3674.

35 R. Rajamanikandan and M. Ilanchelian, *Mater. Sci. Eng., C*, 2019, **98**, 1064–1072.

36 S. S. Skeeters, A. C. Rosu, Divyanshi, J. Yang and K. Zhang, *ACS Appl. Mater. Interfaces*, 2020, **12**, 50203–50211.

37 S. Chakrabortty, M. Sison, Y. Wu, A. Ladenburger, G. Pramanik, J. Biskupek, J. Extermann, U. Kaiser, T. Lasser and T. Weil, *Biomater. Sci.*, 2017, **5**, 966–971.

38 R. Ghosh, U. Goswami, S. S. Ghosh, A. Paul and A. Chattopadhyay, *ACS Appl. Mater. Interfaces*, 2015, **7**, 209–222.

39 H. Zhang, X. Huang, L. Li, G. Zhang, I. Hussain, Z. Li and B. Tan, *Chem. Commun.*, 2012, **48**, 567–569.

40 R. Gui, J. Sun, X. Cao, Y. Wang and H. Jin, *RSC Adv.*, 2014, **4**, 29083–29088.

41 C. Wang, S. Shu, Y. Yao and Q. Song, *RSC Adv.*, 2015, **5**, 101599–101606.

42 H. Miao, D. Zhong, Z. Zhou and X. Yang, *Nanoscale*, 2015, **7**, 19066–19072.

43 T. Zhao, X. W. He, W. Y. Li and Y. K. Zhang, *J. Mater. Chem. B*, 2015, **3**, 2388–2394.

44 Y. Huang, W. Liu, H. Feng, Y. Ye, C. Tang, H. Ao, M. Zhao, G. Chen, J. Chen and Z. Qian, *Anal. Chem.*, 2016, **88**, 7429–7434.

45 J. Liu, Q. M. Zhang, Y. Feng, Z. Zhou and K. Shih, *ChemPhysChem*, 2016, **17**, 225–231.

46 C. Wang, L. Ling, Y. Yao and Q. Song, *Nano Res.*, 2015, **8**, 1975–1986.

47 Y. Luo, H. Miao and X. Yang, *Talanta*, 2015, **144**, 488–495.

48 X. Jia, J. Li and E. Wang, *Small*, 2013, **9**, 3873–3879.

49 X. Jia, X. Yang, J. Li, D. Li and E. Wang, *Chem. Commun.*, 2014, **50**, 237–239.

50 L. Kong, X. Chu, W. Liu, Y. Yao, P. Zhu and X. Ling, *New J. Chem.*, 2016, **40**, 4744–4750.

51 A. Ganguly, I. Chakraborty, T. Udayabhaskararao and T. Pradeep, *J. Nanopart. Res.*, 2013, **15**, 1522.

52 X. G. Li, F. Zhang, Y. Gao, Q. M. Zhou, Y. Zhao, Y. Li, J. Z. Huo and X. J. Zhao, *Biosens. Bioelectron.*, 2016, **86**, 270–276.

53 D. Li, Z. Chen, Z. Wan, T. Yang, H. Wang and X. Mei, *RSC Adv.*, 2016, **6**, 34090–34095.

54 N. Singh, K. P. Raul, A. Poulose, G. Mugesh and V. Venkatesh, *ACS Appl. Bio Mater.*, 2020, **3**, 7454–7461.

55 S. Maity, D. Bain and A. Patra, *J. Phys. Chem. C*, 2019, **123**, 2506–2515.

56 P. Mukherjee, A. Kumar, K. Bhamidipati, N. Puvvada and S. K. Sahu, *ACS Appl. Bio Mater.*, 2020, **3**, 869–880.

57 D. Li, Y. Zhao, Z. Chen, X. Mei and X. Qiu, *Mater. Sci. Eng., C*, 2017, **78**, 653–657.

58 K. Basu, S. Paul, R. Jana, A. Datta and A. Banerjee, *ACS Sustainable Chem. Eng.*, 2019, **7**, 1998–2007.

59 J. Xu and B. Han, *Nano*, 2016, **11**, 1650108.

60 Q. Du, X. Hu, X. Zhang, H. Cao and Y. Huang, *Anal. Methods*, 2019, **11**, 3446–3451.

61 K. Giannousi, K. Lafazanis, J. Arvanitidis, A. Pantazaki and C. Dendrinou-Samara, *J. Inorg. Biochem.*, 2014, **133**, 24–32.